



STRUCTURALLY MODIFIED BIOPOLYMER NANOCOMPOSITE FOR THE PHOTOCATALYTIC DEGRADATION OF METHYLENE BLUE DYE

T. Uma Rajalakshmi*^{1,3}, T. Anantha kumar², G. Alagumuthu³

¹PG and Research Department of Chemistry, Rani Anna Government College for Women, Tirunelveli (affiliated to Manonmaniam Sundaranar University, Abishekapatti, Tirunelveli), Tamil Nadu, India

²Department of Chemistry, Merit Arts and Science College, Idaikal, Ambasamudram, (affiliated to Manonmaniam Sundaranar University, Abishekapatti, Tirunelveli), Tamil Nadu, India

³PG & Research Department of Chemistry, Sri Paramakalyani College, Alwarkurichi (affiliated to Manonmaniam Sundaranar University, Abishekapatti, Tirunelveli), Tamil Nadu, India

*Corresponding author: ananthspkc@gmail.com

Received: 24-09-2021; Revised: 17-02-2022; Accepted: 13-03-2022; Published: 30-04-2022

© Creative Commons Attribution-NonCommercial-NoDerivatives 4.0 International License <https://doi.org/10.55218/JASR.202213310>

ABSTRACT

Environmental pollution, especially water pollution, is a serious problem faced by the world nowadays. Dyes from the textile industry are one of the main causes of water pollution. One of the most widely used methods to reduce dyes pollution is the photocatalytic degradation method. In this paper, structurally modified biopolymer nanocomposites were synthesized by simple precipitation method. The obtained nanocomposites were characterized by X-ray diffraction (XRD), Scanning Electron Microscopy (SEM), Energy Dispersive X-ray Analysis (EDAX), Atomic Force Microscopy (AFM), Transmission Electron Microscopy (TEM), UV-vis absorption spectroscopy and FTIR. The XRD results indicated the nanocomposites are highly crystalline, having the hexagonal wurtzite structure. The particle size can be calculated from the Debye scherrer's formula. The optical properties are studied by UV-visible absorption spectroscopy. In addition, the photocatalytic activity was investigated against methylene blue dye. A good photocatalytic activity was observed from zinc oxide doped biopolymer nanocomposites.

Keywords: Zinc oxide, Biopolymer, Nanocomposites, Methylene blue, Photocatalytic activity.

1. INTRODUCTION

In recent years, development of inorganic-organic hybrid materials on nanometer scale has received significant attention due to a wide range of potential applications and high absorption in the visible part of the spectrum and high mobility of the charge carriers [1-3]. Numerous metal and metal oxide nanoparticles have been encapsulated into polymers to form nanocomposites (NCs). The NCs exhibit combination of properties like conductivity, electrochemical, catalytic and optical properties facilitating innumerable applications like electro chromic devices, light-emitting diodes, electromagnetic interference shielding, secondary batteries, electrostatic discharge systems, chemical and bio-chemical sensors [4] etc. The polymer composites with conventionally filled were described as the new class of materials which enhances the performance, strength, heat resistance, conductivity of the materials [5]. When inorganic particles were doped in a polymer matrix, it

improves the physical properties of the polymer such as conductivity/resistance [6-7]. The polymer with metal oxide doped nanocomposites dramatically show interest to the researchers due to the surprising hybrid properties derived from the polymer and metal oxide [8-9].

In recent decades, semiconductor nanocrystals have great research attention because of their great potential in opto-electronics and bio-applications [10-12]. The II-VI group semiconductors have been intensively studied due to their unique functions than that of other semiconductors. ZnO is a well known semiconductor because of its unique optical and bio-compatible properties that possess huge advantages over other counterparts as a better candidate for bio-applications [13-14]. Among the various nanocrystalline materials, ZnO with particle size in the range of several nm are treated as exclusively suitable material for various applications because of their unique properties [15]. ZnO nanostructures have a wide band gap of 3.37eV and

excitation binding energy of 60MeV [16-18]. In order to tune the size, shape and properties of ZnO, various synthetic methods have been adopted [19-22]. Various synthetic pathways can be adopted for the synthesis of ZnO in many shapes and particle sizes [23-25]. Various synthetic approaches, including hydrothermal [26-28], solvothermal methods [29-31], microemulsion [32], sol-gel method [33], and thermal decomposition of precursors [34-35] have already been reported in the literature. These chemical processes are efficient methods for the preparation of nanoparticles in large scale [36-37].

Dyes, especially methylene blue, are mainly used in the textile, paper, synthetic leather and food industry due to high chemical stability. Effluents containing dyes are discharged into water leading to very serious environmental problems such as mutagenic and carcinogenic to humans and aquatic organisms. Many proposed methods of environmental decontamination involve oxidation of the organic pollutants [38]. Using semiconductor photocatalysts to oxidize and remove such pollutants from water has many advantages over other alternative methods [39]. ZnO nanomaterials are nontoxic and allow very little harm to the environment in which they are used, contrary to most other methods of decontamination. However, there is a little concern about the dissolution of ZnO nanoparticles resulting in Zn toxicity in marine environments [40]. Furthermore, ZnO photocatalysts need not be re-activated after undergoing photoinduced oxidation and reduction reactions. Conversely, activated carbon, a popular choice for water purification, requires costly and potentially polluting reactivation. This paper reports the synthesis of structurally modified nanocomposites using ZnO doped biopolymer nanomaterials. Structural, morphological, optical properties and photocatalytic activity of zinc oxide doped carboxy methyl cellulose biopolymer nanocomposite was studied against methylene blue dye.

2. MATERIAL AND METHODS

The procedures for the synthesis of ZnO nanoparticles and ZnO doped CMC nanocomposite are briefly summarized below. $Zn(NO_3)_2$, $(NH_4)_2CO_3$, sodium hydroxide, ethanol, and de-ionized water were used in the experiments. All the reagents used in this study were of analytical grade.

2.1. Synthesis of ZnO nano particles

$Zn(NO_3)_2$ and $(NH_4)_2CO_3$ were dissolved in high-purity water to form solutions of 1.5 and 2.25 mol/L concentrations respectively. The $Zn(NO_3)_2$ solutions

were slowly dropped into the $(NH_4)_2CO_3$ solutions under vigorous stirring in a magnetic stirrer for 2 hours. The precipitate derived from the above reaction was collected by filtration and rinsed three times with high-purity water and ethanol, respectively. The precipitate was then dried at 80°C to form the precursors ZnO. Finally, the precursors were calcined at a temperature of 500°C for 2 hr in the muffle furnace to obtain the nano-sized ZnO particles.

2.2. Synthesis of ZnO doped CMC nanocomposite

Calculated quantities of the precursor ZnO nanoparticles thus prepared by the above procedure was mixed with 50ml of a solution containing Carboxy methyl cellulose by the continuous dripping of sodium hydroxide from a burette and stirred uniformly in a magnetic stirrer for about 6 hours. The obtained mixture was poured in an autoclave coated with Teflon lining maintained at 180°C for 12 hours filtered, washed with ethanol and water & dried at 80°C for 2 hours so as to obtain the ZnO doped CMC nanocomposite.

2.3. Characterization Techniques

The nanocomposites are generally characterized by their size, morphology and shape. By using the advanced techniques such as X-ray Diffraction (XRD), Scanning electron Microscopy (SEM), Transmission Electron Microscopy (TEM) and Atomic Force Microscopy (AFM). The average particle size, the surface morphology and shape of the nanocomposites were investigated. Fourier Transform Infra Red (FTIR) spectroscopy and UV visible absorption spectroscopy were also performed.

2.3.1. X-ray diffraction

Using XRD, the particle size, nature of the compound, crystal planes and crystalline phases can be evaluated. Each phase exhibits peaks at different 2θ values. From the 2θ values one can interpret the exact phase of the sample. X-ray diffraction (XRD) studies were carried out for the ZnO doped CMC nanocomposite using a Philips powder X-ray diffractometer (Model: PW1710). The XRD patterns were recorded in the 2θ range of 10° - 80° with step width 0.02° and step time 1.25 sec using CuK α radiation ($\lambda = 1.5406 \text{ \AA}$). The analyzed material is finely ground and average bulk composition is determined along with the particle size.

2.3.2. UV visible absorption spectroscopy

UV absorption of the synthesized nanocomposites has been performed using shimadazu UV-Vis spectrometer in

the wavelength range of 200-800 nm with 1000 mm quartz cell. The spectrum is plotted for wavelength on X-axis against absorbance on Y-axis.

2.3.3. Fourier Transform Infra red Spectroscopy

Fourier Transform Infra Red (FTIR) spectroscopy is a very powerful technique which uses electromagnetic radiation in the infrared region for the determination and identification of molecular structure as well as having various quantitative applications within analytical chemistry. FTIR spectra (Model: Perkin Elmer 100) for the ZnO doped CMC polymer nanocomposite was studied in the frequency range of 400 - 4000 cm^{-1} .

2.3.4. Scanning Electron Microscopy

Scanning electron microscopy (SEM) gives morphological examination with direct visualization. SEM of ZnO doped CMC nanocomposite was carried out using scanning electron microscopy (SEM Model: JEOL JSM 6360) operating at 20 kV.

2.3.5. High resolution transmission electron microscopy (HRTEM)

The surface characteristics of the sample are obtained from HRTEM which was performed for ZnO doped CMC nanocomposite using a JEOL JEM-3100F model transmission electron microscope.

2.3.6. Atomic Force Microscopy (AFM)

Atomic force microscopy (AFM) offers ultra-higher resolution in particle size measurement and is based on physical scanning of samples at sub-micron level using a probe tip of atomic scale. The topological study of ZnO doped CMC nanocomposite was carried out using atomic force microscopy (AFM Model: multimode V8).

2.4. Photocatalytic Activity

The photocatalytic activity of the ZnO doped CMC nanocomposite was evaluated by photocatalytic degradation of an aqueous solution of MB (Methylene blue) textile dye under direct sunlight irradiation. The photocatalytic experiments were carried out with 100 mL solution of dye [5×10^{-5} M] and 20 mg of the catalyst at a constant pH 12 under constant stirring. About 3 mL of the aliquot solution was withdrawn at regular time intervals (0-120 min) from the reaction mixture, centrifuged and the decrease in absorbance values was measured. A control experiment was also carried out under identical experimental conditions using commercial MB without catalyst.

$$\% \text{ Decolourization} = [(C_0 - C) \div C_0] \times 100$$

Where, C_0 is the initial concentration of dye solution, C is the concentration of dye solution after photocatalytic degradation.

3. RESULTS AND DISCUSSION

3.1. XRD Analysis

The crystalline structure and particle size of ZnO doped biopolymer nanocomposite were determined using XRD pattern and their corresponding patterns are shown in fig. 1. All the indexed peaks in the obtained spectrum are well matched with that of nanosized zinc oxide (JCPDS file no. 36-1451), confirming the hexagonal wurtzite structure with high purity. The different peaks are obtained along the (100), (002), (101), (102) and (110) planes. The information about the particle size of ZnO doped biopolymer nanocomposite has been obtained from the following Scherrer relations.

$$D = 0.94\lambda / \beta \cos\theta \quad \text{----- (1)}$$

Where D is the average particle size, λ is the wavelength of incident X-ray (1.5418 \AA), β is the full width half maximum (FWHM) of X-ray and θ is the position of the diffraction peak in the diffractogram. The particle size is found to be 41.5 nm.

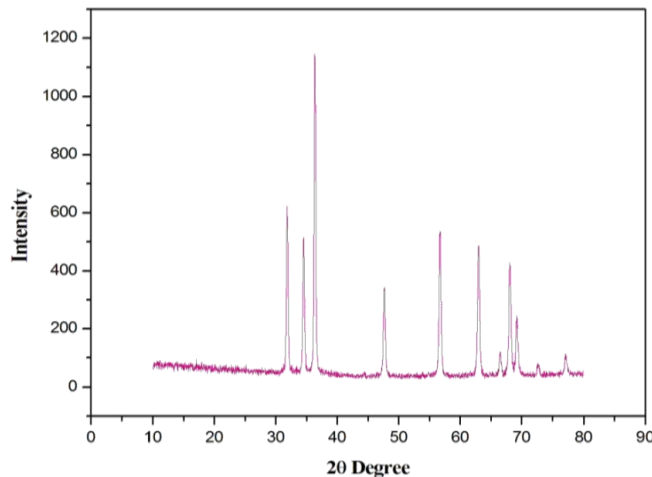


Fig. 1: XRD spectrum of ZnO doped CMC nanocomposites

3.2. SEM with EDAX Analysis

Scanning Electron Microscope was used to identify the surface morphology of the synthesized zinc oxide doped carboxy methyl cellulose nanocomposite on a nanoscale. This picture confirms the formation of zinc oxide doped carboxy methyl cellulose biopolymer nanocomposite and it suggests that the nanocomposite has spherical morphology. From the fig.2, it can be seen that the size

of the metal oxide doped biopolymer nanocomposite was less than 50 nm which was in good agreement with the grain size 41.5 nm as calculated from Debye - Scherrer formula of XRD.

The EDAX spectrum of zinc oxide doped carboxy methyl cellulose nanocomposite is shown in Fig.3. The peaks are corresponding to Zn, O, Na and C are clearly observed in the EDAX spectra at their normal energy and the results clearly indicate the formation of zinc oxide doped carboxy methyl cellulose nanocomposite.

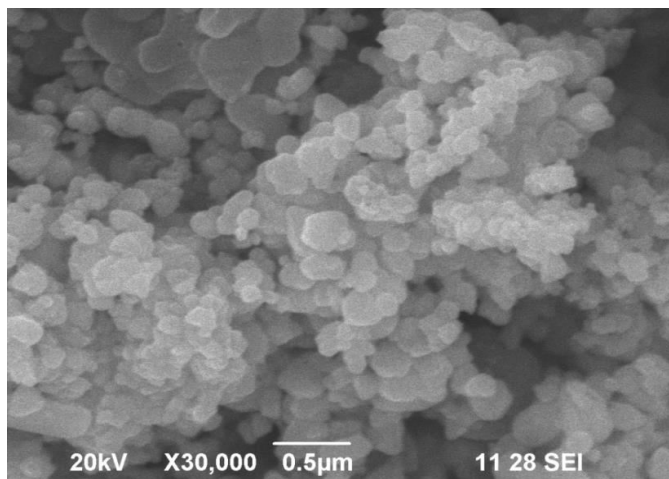


Fig. 2: SEM image of ZnO doped CMC nanocomposites

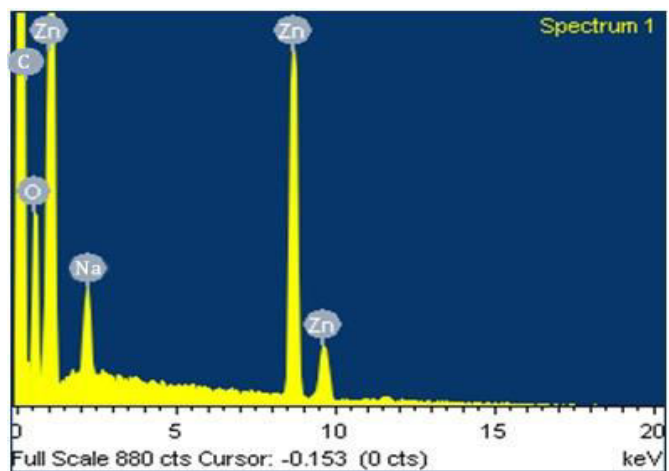


Fig. 3: EDAX spectrum of ZnO doped CMC nanocomposites

3.3. AFM Analysis

Fig. 4 shows the 2D images of the synthesized zinc oxide doped carboxy methyl cellulose nano-composite. The Atomic force microscopy was used to identify the topology and the size range was found to be around 87.2 nm rendering 3D profile. However, the maximum

surface particle size of the ZnO doped CMC nanocomposite lie within 45 nm. Surface roughness, porosity and dimension were also evaluated from AFM image.

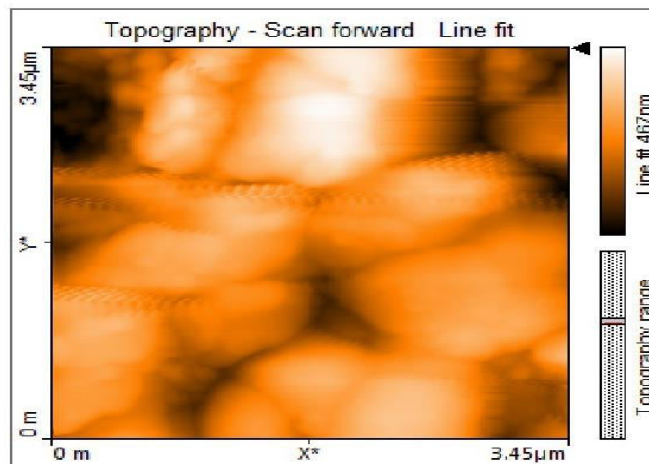


Fig. 4: AFM (2D) image of ZnO doped CMC nanocomposites

3.4. TEM Analysis

The synthesized zinc oxide doped carboxy methyl cellulose biopolymer nanocomposite was further characterized by transmission electron microscope. The shape and particle size of the sample was investigated using TEM analysis. The TEM images of zinc oxide doped carboxy methyl cellulose biopolymer nanocomposite obtained from simple method is shown in Fig. 5. The particle size of the synthesized ZnO nanocomposite was found to be in the range of 30-50 nm. It can be observed that ZnO nanoparticles are present as spherical granules which are well crystallized and embedded in the CMC matrix.

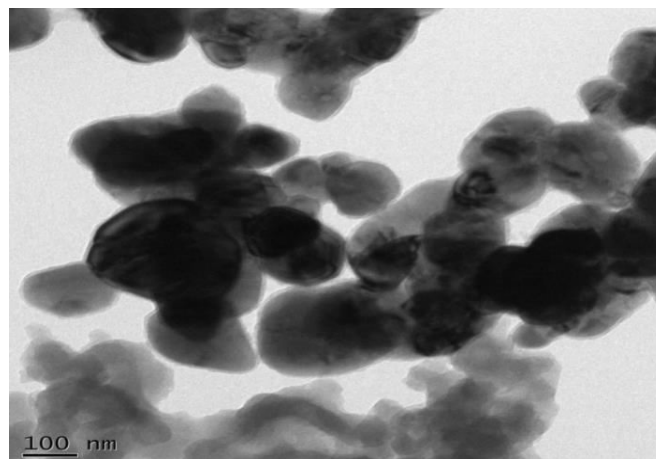


Fig. 5: TEM image of ZnO doped CMC nanocomposites

3.5. Optical Analysis

The optical property of the zinc oxide doped carboxy methyl cellulose nanocomposite was analyzed by UV-Vis absorption spectroscopy at room temperature in the wavelength range between 200 and 800 nm as shown in the Fig. 6. The classical relation for near edge absorption of semiconductors [41] was utilized. The size of the nanocomposites plays an important role in changing the entire properties of the nanomaterials as the semiconducting nanoparticles becomes very essential to explore the properties of the materials. UV-visible absorption spectroscopy is a widely used technique to examine the optical properties of nanosized materials [42]. The UV-Vis absorption spectrum of the synthesized nanocomposite exhibits a strong absorption band at about 325 nm which can be assigned to the intrinsic band-gap absorption of ZnO.

3.6. FTIR Analysis

FTIR spectrum of the synthesized zinc oxide doped carboxy methyl cellulose nanocomposite is given in the Fig.7. The absorption band at 438 cm^{-1} corresponds to the hexagonal wurtzite type ZnO. The appearance of a broad band at 3431 cm^{-1} corresponds to the stretching vibration of O-H groups indicating that the O-H complexes are associated with different defects and

increased free-carrier concentration [41]. A mild absorption band at 1384 cm^{-1} may be either due to the existence of unreacted zinc nitrate [43-44] or due to the carbonate moieties which is generally observed when FT-IR samples are measured in air [45]. The vibrational modes observed at 2854 and 2924 cm^{-1} and that at 1628 cm^{-1} correspond to the stretching vibrations of C-H and C=O of COOH group attributed to the CMC moiety.

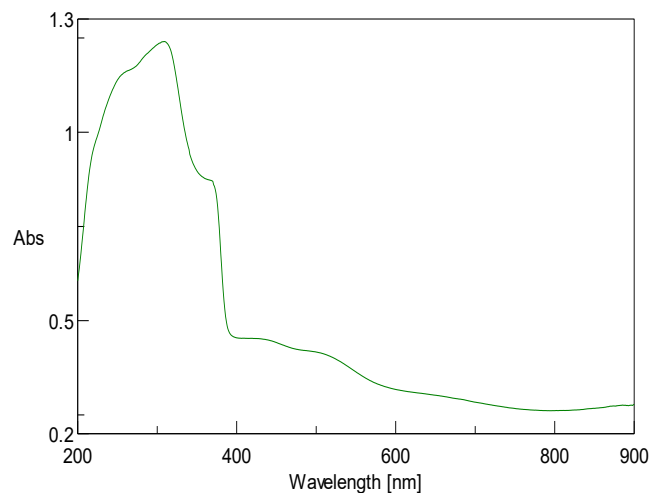


Fig. 6: UV-Vis absorption spectra of the ZnO doped CMC nanocomposites

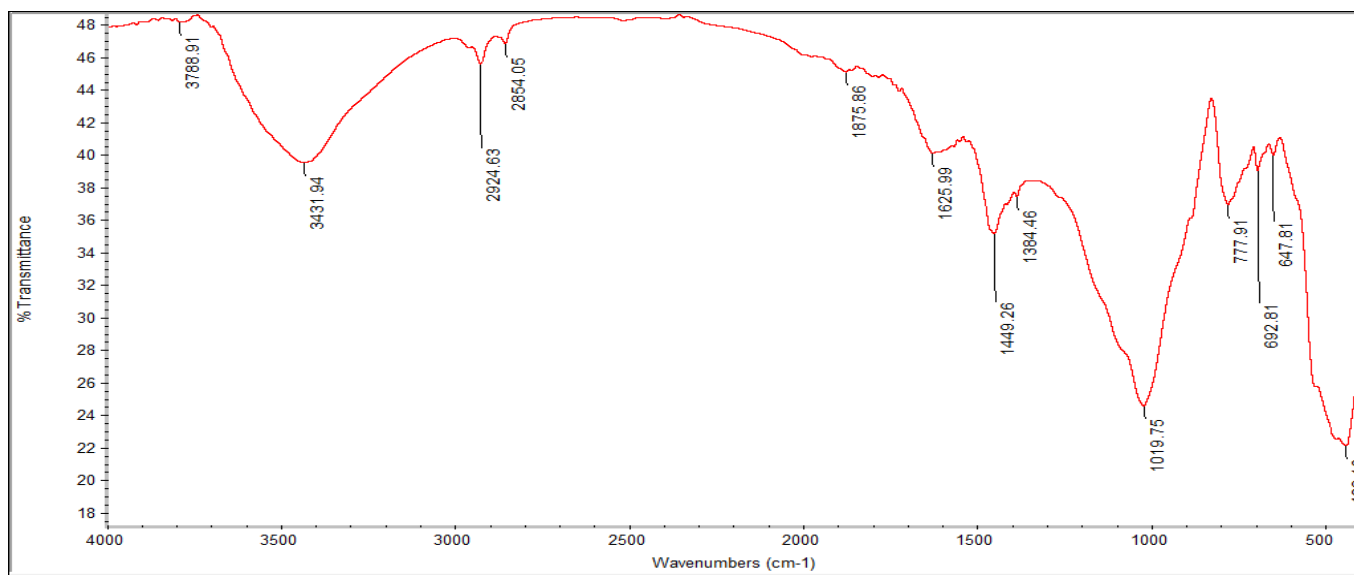


Fig. 7: FTIR spectra of the ZnO doped CMC nanocomposites

3.7. Photocatalytic Activity

The photocatalytic degradation studies have been performed by the degradation of methylene blue dye in aqueous solution under direct sunlight. The zinc oxide

doped carboxy methyl cellulose biopolymer nanocomposite was used as a photocatalyst for the decomposition of the MB dye by the hydroxyl radicals formed at their interface. The absorption at 664 nm was

chosen to monitor the photocatalytic degradation process of MB dye. The degradation of MB dye was visually detected by gradual decrease in the colour from deep blue to colourless solution which was further confirmed by the decrease of the peak intensity at 664 nm during 120 min exposure in direct sunlight as shown in Fig. 8. The kinetic plot of $\ln(A/A_0)$ versus time (T) shows a linear graph suggesting that the degradation follows pseudo first order kinetics with a linear regression coefficient (R^2) 0.988 (Fig.9).

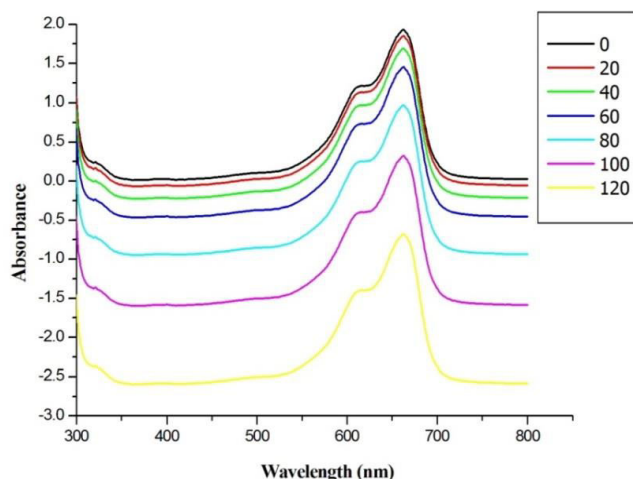


Fig. 8: UV-Vis absorption spectra of methylene blue treated with ZnO doped CMC nano-composites in the photocatalytic reaction

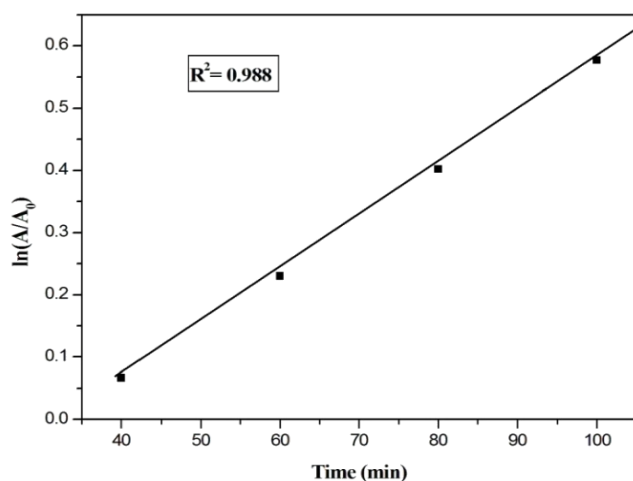


Fig. 9: The kinetic fit for the photocatalytic degradation of MB dye

3.8. Effect of contact time

The contact time plays a crucial role in the photocatalytic degradation of methylene blue (MB) dye. The effects of contact time on the photocatalytic

degradation of MB dye with constant dose of the catalyst (20 mg), pH (12) and initial concentration (5×10^{-5} M) of MB dye was studied. It has been observed from the Fig. 10 that the percentage of photodegradation increases with increase in contact time and complete degradation was achieved within 120 minutes under direct sunlight irradiation. The experimental results showed that the photocatalytic degradation of methylene blue dye obey apparently pseudo first order kinetics and the rate expression is given by the following equation,

$$\ln(C_0/C_t) = k_t t$$

Where, C_0 = initial concentration of dye solution; C_t = concentration of dye solution at various time intervals.

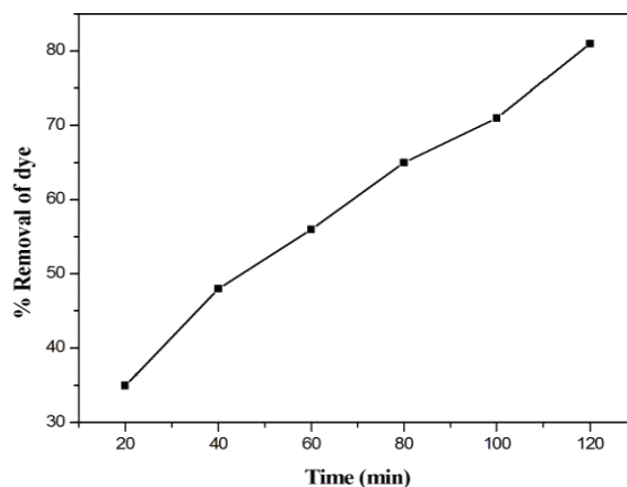


Fig. 10: Effect of contact time

3.9. Effect of catalyst dosage

The photocatalytic degradation of MB dye was observed by varying the amount of catalyst dosage from 10 mg to 20 mg as illustrated in Fig. 11. The increase in the efficiency with the increase of catalyst dosage seems to be due to the increase in the total surface area, namely number of active sites available for the photocatalytic reaction as the dosage of photocatalyst is increased. However, when the photocatalyst was overdosed, the number of active sites on the surface of the photocatalyst may become almost constant due to the decreased light penetration, increased light scattering and loss in surface area caused by the agglomeration at high solid concentration [46-51].

3.10. Effect of initial concentration of dye

The photocatalytic degradation of MB dye was carried out by varying the initial concentrations of the dye from 10 ppm to 50 ppm under direct sunlight. When the

concentration of the dye molecules was increased, the percentage removal was decreased. This is due to the adsorption of excessive dye molecules on the surface of the photocatalyst. Thereby the photon entering pathway may be reduced. This trend of photocatalytic degradation of MB dye is shown in Fig. 12 [52-53].

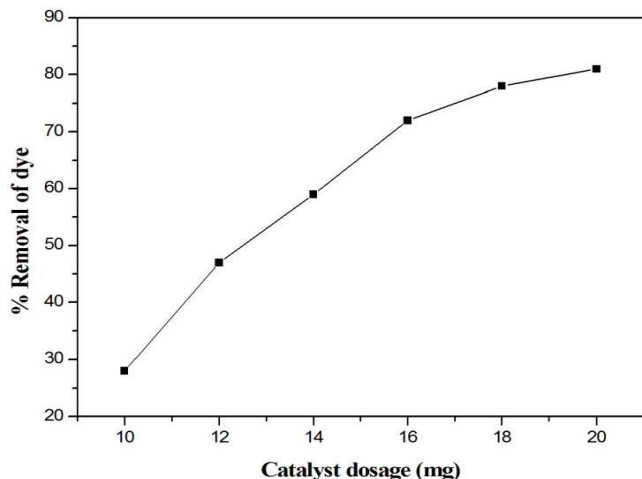


Fig. 11: Effect of catalyst

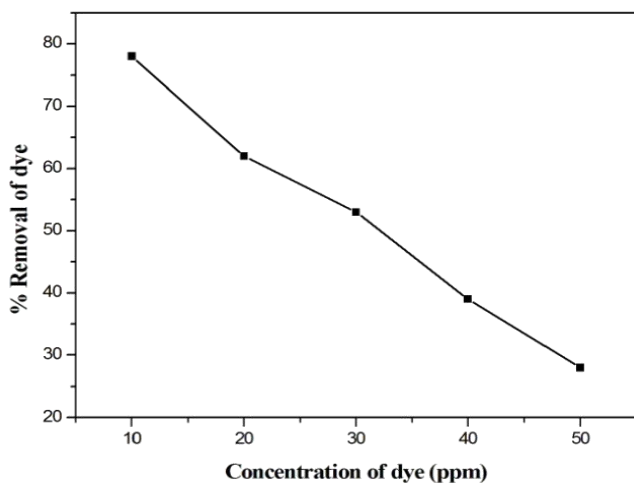


Fig. 12: Effect of concentration of dye

3.11. Effect of pH

The contaminated water from textile industries normally has a wide range of pH values. Hence the experiment was carried out in the pH range 2 to 14 as shown in Fig. 13. The percentage removal of MB increases from 2 to 12 and then becomes almost constant at pH more than 12. This behavior is due to the active sites of CMC carrying a negative charge while the MB carries a positive charge, which causes an electrostatic force of attraction between them and attracts many MB cations from the solution. In contrast, at lower pH, the positive charge increases on CMC, resulting in electronic repulsion with MB cations.

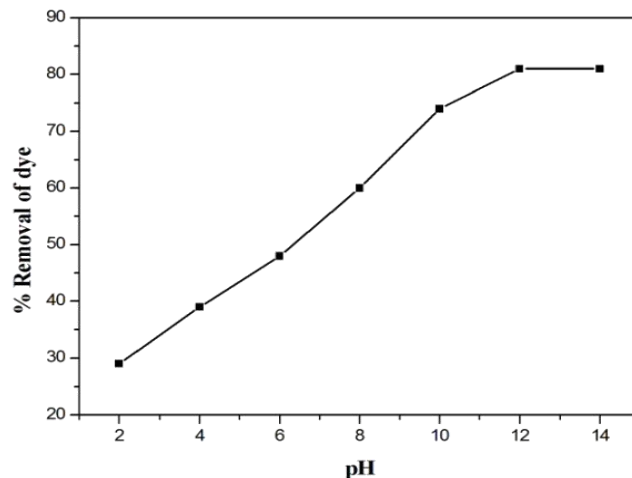


Fig. 13: Effect of pH

4. CONCLUSION

The zinc oxide doped carboxy methyl cellulose nanocomposite was fabricated by a facile method. The synthesized nanocomposite was found to exhibit wurtzite hexagonal structure with high purity. The XRD result proves that the size was approximately 41.5 nm calculated using Debye Scherrer formula. SEM image revealed the spherical morphology for the nanocomposite. The EDX peaks corresponding to Zn, O and C are clearly observed in the EDX spectrum. The shape and size of the sample is inferred from TEM image. The zinc oxide doped carboxy methyl cellulose polymer nanocomposite was found in the range of 30–50 nm. It can be observed that ZnO nanoparticles are present as small granules with spherical shape and are embedded in the biopolymer matrix. The FTIR spectrum confirms the functional groups of zinc oxide doped carboxy methyl cellulose nanocomposites. The UV absorption spectrum of zinc oxide doped carboxy methyl cellulose biopolymer nanocomposite exhibits a strong absorption band at about 325 nm which can be attributed to the intrinsic band-gap absorption of ZnO. Photocatalytic activity studies were performed effectively on MB dye and 80% removal was achieved with catalytic loading of 20 mg at an initial concentration of 10 ppm and an optimum pH 12 in 120 minutes. Based on the above analysis, the resulting materials are found to be very useful in waste water treatment.

Conflict of interest

None declared

Source of funding

None declared

5. REFERENCES

- Ameen S, Akhtar MS, Ansari SG, Yang O, Shin HS. *Superlattices Microstruct.*, 2009; **46(6)**:872-880.
- Sathiyarayanan S, Azim SS, Venkatachari G. *Synth. Met.*, 2007; **157(4-5)**:205-213.
- Stejskal J, Sapurina I, Trchova M. *Prog. Polym. Sci.*, 2010; **35(12)**:1420-1481.
- Umare SS, Shambharkar BH, Ningthoujam RS. *Synth. Met.*, 2010; **160(17-18)**:1815-1821.
- Inzelt G. *Conducting polymers-A new era in electrochemistry*, 2nd Ed. Verlag Berlin Heidelberg:Springer Publishers; 2012.
- Gupta N, Sharma S, Mir IA, Kumar D. *J Sci Ind Res.*, 2006; **65**:549-557.
- Hyeonseok Y. *Nanomaterials*, 2013; **3**:524-549.
- Armelin E, Pla R, Liesa F, Ramis X, Iribarren JI, Aleman C. *Corros. Sci.*, 2008; **50**:721-728.
- Gonçalves GS, Baldissera AF, Rodrigues LF, Martini JEMA, Ferreira A. *Synth. Met.*, 2011; **161**:313-323.
- Singh N, Mehra RM, Kapoor A, Soga T. *J. Renew. Sustain. Energy.*, 2012; **4(1)**:013110.
- Rosenthal SJ, Chang JC, Kovtun O, McBride JR, Tomlinson ID. *Chem. Biol.*, 2011; **18**:10-24.
- Jin T, Sun D, Su JY, Zhang H, Sue HJ. *J. Food Sci.*, 2009; **74(1)**:M46-M52.
- Li M, Lv X, Ma X, Sun F, Tang L, Wang Z. *Mater. Lett.*, 2007, **61(3)**:690-693.
- Ratkovich A, Penn RL. *Mater. Res. Bull.*, 2009; **44(5)**:993-998.
- Wang L, Muhammed M. *J. Mater. Chem.*, 1999; **9**:2871-2878.
- Hong R, Pan T, Qian J, Li H. *Chem. Eng. Sci.*, 2006; **119**:71-81.
- Bu IYY. *Ceram.*, 2013; **39**:1189 – 1194.
- Xu H, Wang H, Zhang Y, He W. *Ceram.*, 2004; **30**:93-97.
- Barsan N, Weimar U. *J. Electroceramics.*, 2001; **5**:143 – 167.
- Cho S, Jung H, Hong Lec K. *J. Phys. Chem. C.*, 2008; **112**:12769 – 12776.
- Krishna kumar T, Jayapralash R, Pinna N, Singh VN, Mehta BR, Phani AR. *Mater. Lett.*, 2009; **63**:242-245.
- Yamazoe N, Shimanoe K. *J. Electrochem. Soc.*, 2008; **155**:S85 – S92.
- Demir MM, Munoz-Espi R, Lieberwirth I, Wegner G. *J. Mater. Chem.*, 2006; **16**:2940–2947.
- Bitenc M, Drai G, Orel ZC. *Cryst. Growth Des.*, 2010; **10**:830–837.
- Ambroi G, Djerdj I, Kapin SD, Igon M, Orel ZC. *CrystEngComm.*, 2010; **12**:1862–1868.
- Liu B, Zeng HC. *J. Am. Chem. Soc.*, 2003; **125**:4430–4431.
- Sun XM, Chen X, Deng ZX, Li YD. *Mater. Chem. Phys.*, 2003; **78**:99– 104.
- Bitenc M, Podbrek P, Orel ZC, Cleveland MA, Paramo JA, Peters RM, Strzhemecny YM. *Cryst. Growth Des.*, 2009; **9**:997–1001.
- Yang L, Wang GZ, Tang CJ, Wang HQ, Zhang L. *Chem. Phys. Lett.*, 2005; **409**:337–341.
- Yu SH, Yang J, Quian YT, Yoshimura M. *Chem. Phys. Lett.*, 2002; **361**:362–366.
- Ambroi G, Kapin SD, Igon M, Orel ZC. *J. Colloid Interface Sci.*, 2010; **346**:317–323.
- Guo L, Ji Y, Xu H. *J. Am. Chem. Soc.*, 2002; **124**:14864–14865.
- Mondelaers D, Vanhoyland G, Van den Rul H, Haen J, Van Bael MK, Mullens J, Van Poucke LC. *Mater. Res. Bull.*, 2002; **37**:901–914.
- Wang Z, Zhang H, Zhang L, Yuan J, Yan S, Wang C. *Nanotechnology*, 2003; **14**:11–15.
- Pillai SC, Kelly JM, McCormack DE, Brien PO, Ramesh R. *J. Mater. Chem.*, 2003; **13**:2586–2590.
- Masala O, Seshandri R. *Annu. Rev. Mater. Res.*, 200; **34**:41–81.
- Feng X, Hu MZ. Ceramic nanoparticle synthesis. in 'Encyclopaedia of nanoscience and nanotechnology'. (ed.:Nalwa H. S.):American Scientific Publishers; Vol 1, 2004. P. 687-726.
- Oppenlander T. *Photochemical Purification of Water and Air:Advanced Oxidation Processes (AOPs) - Principles, Reaction Mechanisms, Reactor Concepts*, Wiley-VCH Publisher; 2003.
- Anpo M. *Pure Appl. Chem.*, 2000; **72**:1265–1270.
- Bian S, Mudunkotuwa I, Rupasinghe T, Grassian V. *Langmuir*, 2011; **27**:6059–6068.
- Anantha kumar T, Malathi S, Mythili CV, Jeyachandran M. *Int. J. Chemtech Res.*, 2018; **11(08)**:48-57.
- Satyanarayana T, Srinivasa RK, Nagarjuna G. *ISRN Nanotechnology*, 2012; 1-6.
- Maensiri S, Laokul P, Promarak V. *J. Cryst. Growth*, 2006; **289**:102-106.
- Biswick T, Jones W, Pacu A, Serwick E, Podobinski J. *J. Solid State Chem.*, 2007; **180**:1783-1786.
- Lili W, Youshi W, Yuanchang S, Huiying W. *Rare Met.*, 2006; **25**:68-73.
- Fujishima A, Honda K. *Nature*, 1972; **238(5358)**:37–38.

47. Kudo A, Miseki Y. *Chem. Soc. Rev.*, 2009; **38(1)**:253–278.
48. Tseng YH, Kuo CH. *Catal. Today*, 2011; **174(1)**:114–120.
49. Ismaila AA, Geioushya RA, Bouzid H, AlSayari SA, Al-Hajry A, Bahnemann DW. *Appl. Catal. B.*, 2013; **129**:129–132.
50. Gupta VK, Jain R, Mittal A, Saleh TA, Nayak A, Agarwal S, Sikarwar S. *Mater. Sci. Eng.*, 2012; **32(1)**:12–17.
51. Abo-Farha SA. *Am. J. Sci.*, 2010; **6(11)**:130–142.
52. Devi LG, Kumar SG. *Appl. Surf. Sci.*, 2011; **257(7)**:2779–2790.
53. Hoffmann MR, Martin ST, Choi W, Bahnemann DW. *Chem. Rev.*, 1995; **95(1)**:69–96.